Nanoscale

Cite this: *Nanoscale*, 2012, **4**, 5718

www.rsc.org/nanoscale

PAPER

Facile fabrication of nanofluidic diode membranes using anodic aluminium oxide†

Songmei Wu,* Fabien Wildhaber, Oscar Vazquez-Mena,‡ Arnaud Bertsch, Juergen Brugger and Philippe Renaud

Received 21st May 2012, Accepted 17th July 2012
DOI: 10.1039/c2nr31243c

Active control of ion transport plays important roles in chemical and biological analytical processes. Nanofluidic systems hold the promise for such control through electrostatic interaction between ions and channel surfaces. Most existing experiments rely on planar geometry where the nanochannels are generally very long and shallow with large aspect ratios. Based on this configuration the concepts of nanofluidic gating and rectification have been successfully demonstrated. However, device minimization and throughput scaling remain significant challenges. We report here an innovative and facile realization of hetero-structured Al_2O_3/SiO_2 (Si) nanopore array membranes by using pattern transfer of self-organized nanopore structures of anodic aluminum oxide (AAO). Thanks to the opposite surface charge states of Al_2O_3 (positive) and SiO_2 (negative), the membrane exhibits clear rectification of ion current in electrolyte solutions with very low aspect ratios compared to previous approaches. Our hetero-structured nanopore arrays provide a valuable platform for high throughput applications such as molecular separation, chemical processors and energy conversion.

Introduction

Novel ion transport properties emerge in nanofluidic systems owing to the high surface to volume ratio of nanochannels. When at least one dimension of a nanochannel is comparable to the ion screening length known as the Debye length (*i.e.* length of the electrical double layer), the channel becomes selective to counterions (*i.e.* ions of opposite charge polarity relative to surface charges of channel walls) due to the overlapping of electrical double layers. The Debye length λ is proportional to $1/\sqrt{c_{bulk}}$ (c_{bulk} being the bulk ionic concentration) and ranges typically between 1 and 100 nm in aqueous solution. In such a polarized ion channel, the average concentration of counterions $c_{counter}$ in a nanopore with radius r is governed by the surface charge density of channel walls: $c_{counter} = 2q/rF$, F being the Faraday constant and q being the surface charge density of the nanopore surface.[1–3] It is therefore possible to control the concentration of counterions inside nanochannels by modulating the surface potential of the channel walls. For instance, a metal electrode can be embedded inside a dielectric layer, with which the surface potential of the channel walls can be tuned by an external electric field. Such a configuration can be used to control the polarity and concentration of ions within the nanochannel in a manner similar to a semiconductor transistor.[4–8] Another basic element for controlling ion transport aims at controlling the direction of ion flow, analogous to the rectification behavior of a semiconductor diode. Such kind of behavior has been previously observed in bipolar ion exchange polymer membranes[9–12] and recently predicted in theory[13–15] and demonstrated in nanofluidic systems.[16–25] The key challenge to realize these devices is to create asymmetric distribution of surface potential and charge carriers inside the channel. This asymmetry can be achieved by geometry, surface charges, differential concentrations or pressures in electrolyte reservoirs.

To date, the majority of active nanofluidic devices are based on planar channels which are generally very long and shallow with large aspect ratios. The nanometer limiting dimension, which is normally the channel height, is defined by the thickness of a sacrificial silicon layer while the channel width and length vary from micrometers to millimeters. Based on the "etching followed by bonding" scheme, various types of experiments have been carried out to demonstrate the principle of ionic and molecular transport in one or several nanochannels.[4,26,27] More sophisticated nanofluidic devices can be obtained by first synthesizing and then contacting mesoporous materials or single nanotubes, generally with a complex process flow.[7,21] Recent developments in nanotechnologies such as FIB (Focused Ion Beam) and high

Microsystems Laboratory, École Polytechnique Fédérale de Lausanne, EPFL STI-IMT-LMIS, Station 17, 1015 Lausanne, Switzerland. E-mail: songmei.wu@epfl.ch

† Electronic supplementary information (ESI) available: Pattern transfer of local AAO mask into Si layers of different thickness; characterization of the Ag/AgCl electrodes and the cell constant; control experiments of mono-charged nanopore membranes; and simulation of ionic transport in nanofluidic diodes. See DOI: 10.1039/c2nr31243c

‡ Current address: Department of Physics, University of California at Berkeley, California 94720, USA.

resolution e-beam lithography allow the fabrication of solid state single nanopores or nanopore arrays with controlled precision down to a few nm.[21,28–30] However, they are not suitable for large scale application due to their serial nature.

We present here a facile realization of hetero-structured nanopore membranes for nanofluidic diodes. The membrane is composed of Al_2O_3 and SiO_2(Si) layers with dense nanopore arrays as shown in Fig. 1a. SiO_2(Si) denotes the native dioxide layer of Si. The average pore diameter is typically 20 nm and the thickness of the membrane is several hundred nanometers. On exposure to aqueous solution, the oxides become hydrated and the surface charge state of the oxide is determined by the dissociation of hydroxyl groups. In pH-neutral solutions, Al_2O_3 surfaces possess net positive charges: Al–OH + H^+ ↔ Al–OH_2^+, while native dioxide layers of Si possess net negative charges: SiOH ↔ SiO^- + H^+.[31,32] The advantage of our geometry is that the surface area just outside the nanopore has the same charge polarity and charge density as the corresponding internal side of the nanopores, which can enhance the ion selectivity in the nanopores. A single nanofluidic diode nanopore is illustrated in Fig. 1b. In low concentration electrolytes where the electrical double layer of pore surfaces overlaps, the hetero-structured nanopores attract counterions as major charge carriers inside the electrical double layer, *i.e.* negative ions (Cl^-) at Al_2O_3 side and positive ions (K^+) at SiO_2(Si) side, forming a large parallel array of very low aspect ratio nanofluidic diodes. At reverse bias, counterions are driven away from the junction. As a result, the ionic current ceases because a depletion region is created in the nanopores. In contrast, at forward bias, both ions are driven towards the junction and ion enrichment occurs. A continuous ion current can therefore be maintained across the nanopores. The membrane configuration ensures a high throughput property since there are many parallel nanochannels with low aspect ratios. The performance of the device is further improved by the same charge polarity and density on membrane surfaces near the nanochannels. The realization of the hetero-structured Al_2O_3/SiO_2(Si) nanopore membrane, as we shall see, is a scalable and cost efficient bottom-up approach based on self-organized nanopore structures in anodic aluminum oxide (AAO) followed by a pattern transfer process.

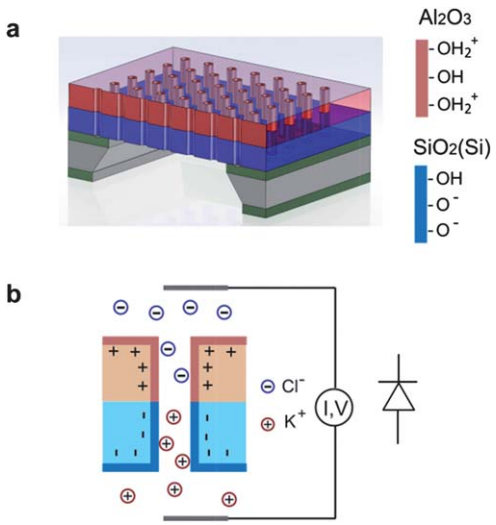

Fig. 1 Schematic of a solid state ionic diode nanomembrane. (a) The nanopore array membrane is composed of two layers carrying opposite surface charges: –OH_2^+ on the top Al_2O_3 layer and –O^- on the bottom SiO_2(Si) layer. SiO_2(Si) denotes the native oxide layer of Si. (b) Illustration of a single nanofluidic diode nanopore. In low concentration electrolytes, the nanopore is selective to counterions (*i.e.* ions of opposite charge polarity relative to the surface charges of the nanopores). The nanopore with asymmetric surface charges can therefore function as a nanofluidic diode. The surface of the membrane possesses similar charge polarity and density to those on the corresponding internal walls of the nanopores, which facilitates the charge selectivity in the nanopores by forming pre-concentration conditions.

Results and discussion

Fabrication of hetero-structured Al_2O_3/SiO_2(Si) nanopore membrane

The fabrication process is summarized in Fig. 2. Standard microfabrication tools are used to define the size of the free standing low stress silicon nitride (LS SiN) membranes which serve as supporting layers for further processing. 250 nm of amorphous silicon and 150 nm of Al layers are then deposited on the LS SiN membranes (Fig. 2a). The area of the membrane is typically 200 × 200 μm^2. Anodization of Al creates self-organized nanopore structures (Fig. 2b). Owing to its relatively easy and cost-efficient processing anodic aluminum oxide has been used extensively as a template for fabrication of low dimensional nanostructures including direct growth of nanowires inside nanopores and pattern transfer to various substrates.[33–38] We explore here the formation of hetero-structures of Al_2O_3/SiO_2(Si) through Cl_2 RIE (Reactive Ion Etching) of the Si underlayer by using very thin porous alumina as a local etch mask (Fig. 2c). The pore size and aspect ratio of top Al_2O_3 nanopores as well as the thickness of the bottom Si layer are optimized in order to achieve proper pattern transfer with small pore diameters. Finally the diode membrane is released by selective dry etching of the LS SiN supporting layer (Fig. 2d).

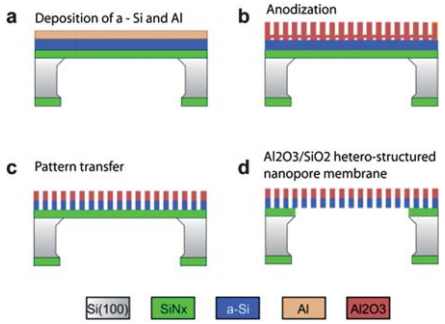

Fig. 2 Fabrication process flow of an ionic diode nanomembrane. (a) Amorphous silicon and aluminum thin layers are deposited on a low stress silicon nitride (LS SiN) supporting membrane. (b) Self-organized alumina nanopores are created by anodization of aluminum. (c) Alumina nanopore structures are transferred into the silicon layer by reactive ion etching, forming hetero-structured Al_2O_3/SiO_2(Si) nanopore arrays. (d) Final release of the hetero-structured nanopore membrane by selective etching of the LS SiN supporting layer.

The characterization of a hetero-structured membrane is shown in Fig. 3. Fig. 3a contains an SEM (Scanning Electron Microscope) image of the top alumina layer and the histogram of pore diameters. The structures are featured after anodization, pore opening and Cl_2 plasma etching (see Methods). The pore diameter is 22 ± 5 nm, corresponding to a pore density of about 400 μm^{-2}. As the result of anodization of a very thin Al film (150 nm), the nanopores reveal only pseudo-hexagonal pattern and there are size and shape distributions. The regularity and homogeneity of the pores can be further improved by pre-patterning methods such as nano-indentation on Al surface which can guide the growth of nanopores during anodization.[39] The bottom image of the membrane shown in Fig. 3b, however, is very different compared to the top one. The number of open pores in the Si layer is much less and the pore arrangement is more random. The pore diameter is 18 ± 7 nm and pore density is around 8 μm^{-2}, meaning that about 2% of the top pores are transferred to the bottom Si layer. The porosity of the diode membrane can be modulated by plasma etching conditions and thickness of the Si layer. The same etching conditions lead to higher porosity and larger pore diameters in thinner Si layers. The transferred patterns are compared in the ESI Fig. S1.† The cross-section image and 3D profile of the nanopores in Fig. 3c and d obtained by FIB and SEM investigations provide an inside view of the hetero-structures. For the operation of FIB and SEM imaging, 20 nm of Pt was deposited by ALD (Atomic Layer Deposition) to conformally coat the nanochannels. The alumina nanopores exhibit a cylinder shape which is well defined by anodization. It is also clearly seen that not all the pores initiating from the surface can finally reach the bottom. This is the consequence of the typical branching or pore regulation progress occurring for anodization of a thin Al film. The following Cl_2 RIE etches both alumina and Si with a selectivity of about 1 : 8 for bulk materials. The etching process mills away a thin layer of alumina and slightly enlarges the pores from the top. After removing a barrier layer at the bottom of the alumina layer, the plasma reaches the Si layer. The etching to Si is anisotropic hence the Si channels maintain the cylindrical feature, although the profile is generally rougher than that of anodized alumina channels. The 3D profile reveals that only a small proportion of the channels open through the bottom of the Si layer, as a consequence of the size distribution in the top mask. We think that the pores in the bottom Si layer are mainly transferred by the large pores from the top alumina side. Due to the small interpore distance in the alumina mask, there could also occur merging of neighboring pores in the Si layer at the position close to the interface.

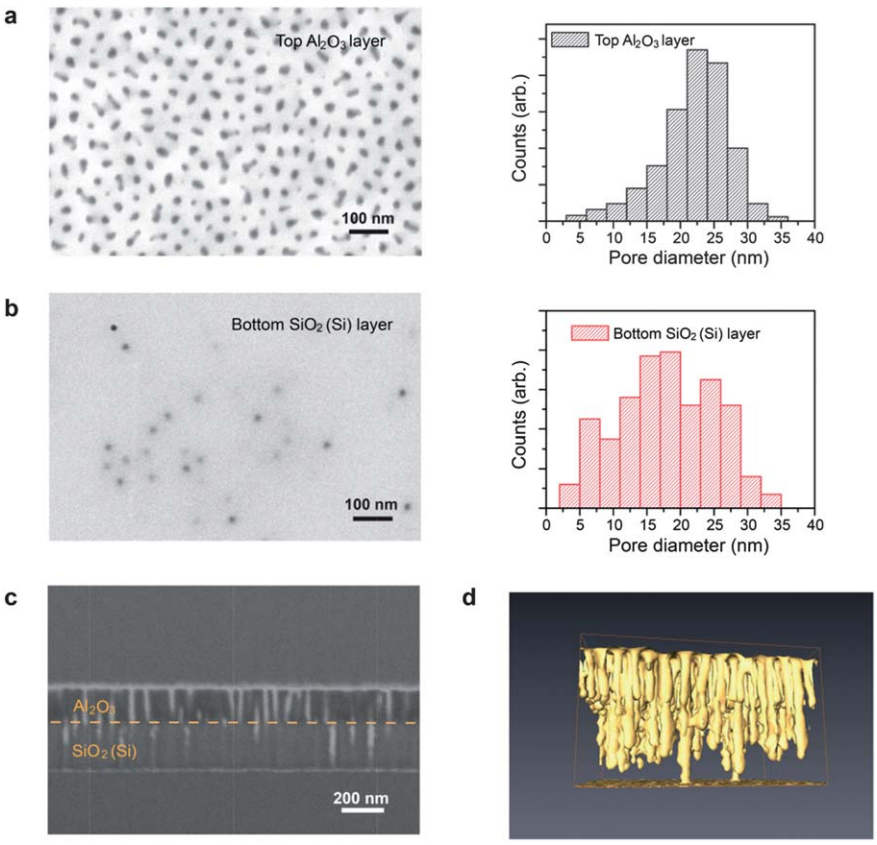

Fig. 3 Sample characterization of a very low aspect ratio Al_2O_3/SiO_2(Si) hetero-structured nanopore membrane. (a) An SEM top view of the membrane and histogram of pore diameters. (b) An SEM bottom view of the membrane and histogram of pore diameters. (c) A FIB-SEM cross-section image of the membrane. The nanopores as well as the membrane surfaces are coated conformally with 20 nm Pt by atomic layer deposition which appear bright in the image. The dashed line indicates the interface of the top alumina layer and the bottom Si layer. (d) A 3D picture reconstructed from FIB-SEM investigation representing the profile of the nanopores. The bright bottom layer corresponds to the Pt layer on the membrane.

In summary, the hetero-structured membrane is composed of 150 nm thick alumina layer and 250 nm thick Si layer with native silicon dioxide. The average pore diameter is 20 nm and the aspect ratio of the nanopores is nearly 20 : 1. We hypothesize that the hetero-structured, high density nanopore membranes with such a low aspect ratio behave as nanofluidic diode arrays. Thus, we further characterize the ion transport properties through the membrane.

Characterization of ionic transport through the membrane

The nanofluidic diode behavior of the $Al_2O_3/SiO_2(Si)$ membrane is demonstrated in KCl electrolyte at varied concentrations ranging from 0.1 mM to 2 M. The membrane is inserted between two reservoirs with the same ionic concentration and liquid pressure. A pair of Ag/AgCl electrodes is used to apply a potential through the membrane. The electrodes are fabricated by the anodization of Ag wires in HCl solution. The characterization of the Ag/AgCl electrodes and the cell constant are described in the ESI Fig. S2.† For our liquid cell configuration, low porosity samples (*i.e.* high resistance) as depicted in Fig. 3b are preferred in order to minimize the contribution from cell geometries to ionic current through the membrane.

I–V curves at ionic concentrations ranging from 0.1 mM to 0.1 M (Fig. 4a–d) exhibit clear rectifying effects: the ionic current increases exponentially at forward bias, and there is linear leakage current appearing at reverse bias. The rectifying behavior is expected especially at low ion concentrations where the Debye length is comparable to the pore radius. The average pore radius is 20 nm, and the typical Debye length is 10 nm at 1 mM and 1 nm at 0.1 M, respectively. The rectification phenomenon is clearly visible even when the pore radius is larger than the Debye length at a given ionic concentration. This is because the absolute potential at the solid surface decreases exponentially along the distance from the surface. The increased counterion concentration region in the pores extends much further than the Debye length. A similar phenomenon has been depicted by theory[13] and observed by previous experiments with large aspect ratio nanochannels.[21,23] At high concentrations, the rectification effect diminishes (Fig. 4e and f). In 2 M KCl solutions, the surface charges of channel walls are completely shielded by counterions so that the surface charges no longer influence the ionic transport inside the nanopores, therefore no current rectifying behavior is observed.

The current values extracted at forward (+0.5 V) and reverse bias (−0.5 V) as well as rectification factors at different KCl concentrations (inset) are summarized in Fig. 5. The obvious splitting of conductance at forward and reverse bias occurs at concentrations as high as 0.1 M, indicating the involvement of surface charges of pore walls in ion transport. Another indication of this surface charge dominating transport properties would have been that the conductance of nanopores stays at a constant value at low bulk concentrations. This is because the amount of charge carried in each side of the hetero-structured nanopores is determined by the total charges of pore walls and is therefore independent of bulk concentrations: $c_{counter} = 2q/rF$.

However, such a conductance plateau (at forward bias) does not appear for our membrane device, even though the surface area around the nanopores possesses similar charge polarity and density as those in corresponding internal walls of the nanopores,

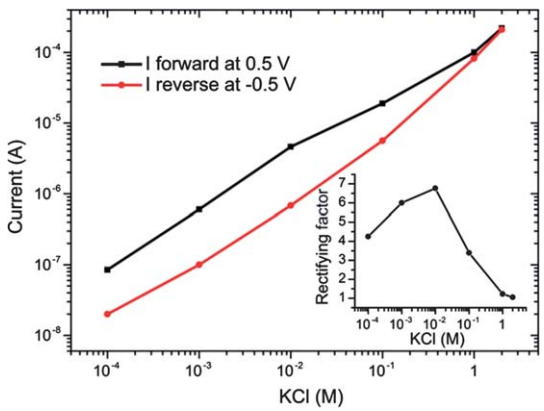

Fig. 5 Log–log plot of current values at +0.5 V forward and −0.5 V reverse bias at different ionic concentrations. Inset: summarized rectifying factors.

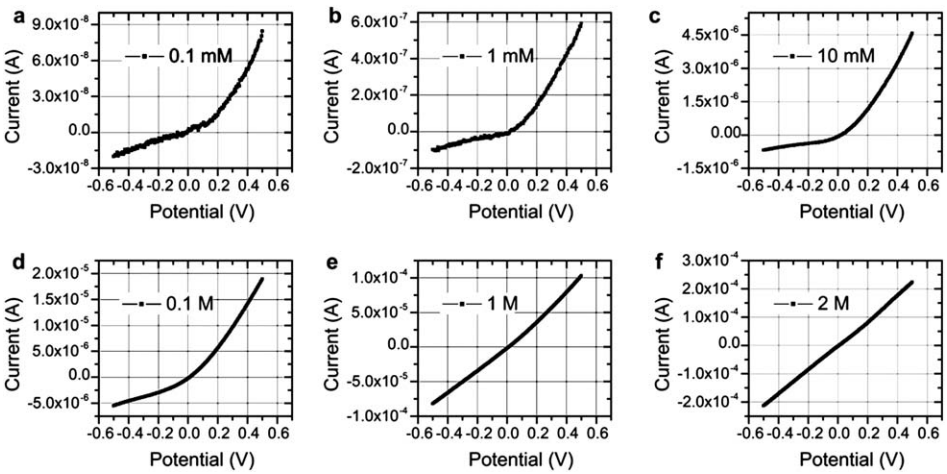

Fig. 4 *I–V* curves of a nanofluidic diode membrane measured in KCl electrolyte at varied concentrations: (a) 0.1 mM; (b) 1 mM; (c) 10 mM; (d) 0.1 M; (e) 1 M; and (f) 2 M.

which should form pre-concentration conditions to facilitate the charge selectivity in the nanopores.[40] The fact that the current values at forward bias scale down with bulk concentrations suggests that a concentration-dependent parameter such as cell constant starts to play a non-negligible role in the total potential drop. In our geometry, the nanopores in the membrane are very short and parallel. At low ionic solutions, the conductance of the nanopores becomes comparable or even smaller than the cell constant. As a result, the conductance curve shows a tendency of linear decay at low bulk concentrations.

Such an effect can be qualitatively explained by a numerical simulation based on the Poisson–Nernst–Planck equation. The nanochannel under consideration is a single nanofluidic diode of 10 nm radius and 400 nm length. It is composed of two surfaces with opposite charge polarities with an absolute value of charge density of 5 mC m^{-2} which is a typical value for native oxides.[23]

The details of the physical model are described in the ESI† and the results are summarized in Fig. 6. For the single diode channel, simulated conductance curve at forward bias exhibits the feature of a plateau at low KCl concentrations (curve 1 with empty circles). Curve 2 (dashed line) reveals the cell conductance at varied ionic concentrations. The difference between the cell conductance and the simulated membrane conductance at 1 M was calculated based on the ratio of experimental values. For the sake of simplicity, the cell conductance is proportional to the concentration of bulk electrolyte without considering the mobility change of ions at different concentrations. For the "single diode channel + cell conductance" system, the cell conductance behaves as a serial conductor. In high concentration electrolytes, the contribution of the cell conductance is negligible, however, it becomes dominating at low concentrations. As a result, the overall conductance curve deviates from calculated feature of a plateau and rather shows a linear behavior (curve 3 with full circle). At reverse bias, the simulated conductance values decay dramatically at low concentrations (curve 4 with empty square). However, if we consider an additional small leakage current (for example, curve 5 dotted line), it leads to the increase of reverse conductance from curve 4 (empty square) to curve 6 (full square). By considering the effect of the cell conductance at forward bias and the leakage current at reverse bias, the overall transport properties (curves 3 and 6 in Fig. 6) tend to be consistent with experimental observations in Fig. 5.

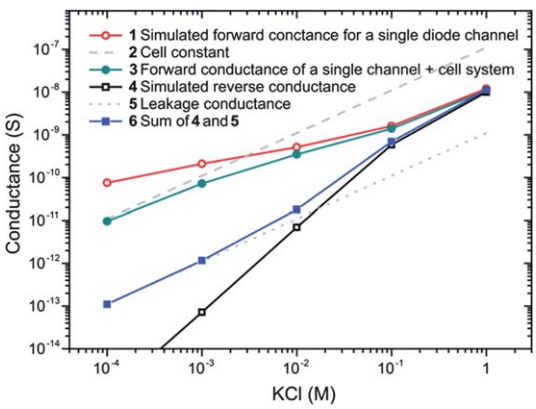

Fig. 6 Numerically simulated transport properties of a single ionic diode channel and the effect of the cell constant at forward bias and leakage current at reverse bias. Curve 1 (empty circle): simulated conductance curve at forward bias showing the feature of a plateau at low KCl concentrations. Curve 2 (dashed line): cell constant. The cell conductance is proportional to the concentration of bulk electrolyte. Curve 3 (full circle): resulted conductance curve for the "single diode channel + cell conductance" system. It shows linear decay with ionic concentrations. Curve 4 (empty square): simulated conductance values at reverse bias. Curve 5 (dotted line): leakage conductance which scales linearly with ionic concentrations. Curve 6 (full square): sum of curves 4 and 5. The overall conductance at reverse bias increases as the result of leakage current.

Although we have observed orders of magnitude higher current values than reported elsewhere for long and shallow planar channels, the rectifying factor shown in Fig. 5 (inset) is relatively low (max. 7). The leakage current is inherent due to the very low aspect ratio (20) of nanopores, as compared to 200 μm alumina/silicon dioxide heterostructured planar channels with an aspect ratio larger than 10 000 where a rectifying factor of 200 was reported.[23] On the other hand, the forward current is very likely under-evaluated as the result of high throughput characteristics of the membrane. The potential drop due to the concentration polarization near the surface of the membrane as well as the cell configuration cannot be neglected. Consequently, the potential bias between the two sides of the membrane becomes smaller than the bias applied between the two ends of the reservoirs. We expect that the performance of our devices can be improved by optimizing the sample geometry. For example, aspect ratios of nanopores can be increased by further shrinking the pore size and a device with smaller porosity should also help to access the signal from the nanopores. Alternatively, instead of amorphous Si, a conducting layer can make the device field addressable that would allow tuning of the diode property by modulating the electric field.

Conclusion

In conclusion, by using pattern transfer of self-organized AAO nanotemplates, we have successfully fabricated alumina/silicon dioxide hetero-structured solid state nanopore membranes. The membrane behaves as a parallel array of nanofluidic diodes, exhibiting rectification of ionic current at relatively high electrolyte concentrations. Although the finite rectification ratios for these devices deviate from the ideal diode characteristics, the development of such hetero-structured nanopore membranes would enable various high throughput applications in nanofluidic chemical processors and molecular separations. The flexibility of this approach lets us envisage the realization of more complex structures with a combination of various metals and oxides, for instance, nanofluidic bipolar transistors.

Methods

Fabrication of hetero-structured nanopore membranes

A 250 nm amorphous Si layer was first sputtered onto a 1 × 1 cm^2 chip with a 200 × 200 μm^2 500 nm thick LS SiN membrane, followed by the evaporation of a 150 nm Al layer. The anodization of the Al thin film was performed in a 3% (v/v) H_2SO_4 solution under 20 V. The anodization process lasts for about 70 s. The thickness of resulted nanoporous alumina became 220 nm, which is about 1.5 times larger than the original thickness of Al.

Then the nanopores were slightly enlarged in a 6% (wt) H_3PO_4 solution for 5 min at a pore opening rate of 0.5 nm min^{-1}. After thoroughly rinsing with DI water, the samples were dried under nitrogen before plasma etching. The RIE (Reactive Ion Etching) process was carried out in an STS Multiplex ICP (Inductively Coupled Plasma) etcher, utilizing 50 sccm Cl_2, RF forward power coil/platen 800/100 W and pressure 5.0 mTorr. The Cl_2 plasma etches both alumina and Si with a selectivity of 1 : 8. After 2 min etching, the patterns of top porous alumina were partially transferred to the Si layer. The porosity and pore profile of the entire device can be modified by tuning the etching time and pore size of the AAO mask. Finally the LS SiN layer was selectively removed in an Alcatel 601E DRIE (Deep Reactive Ion Etching) etcher by using C_2F_6.

Electrical measurement

A potential sweep from −0.5 V to +0.5 V and then back to −0.5 V was applied to the Ag/AgCl electrodes with 0.005 V step and average of 100 points/applied potential. Measurement of one cycle took about 20 s. The *I–V* curves shown in Fig. 4 were obtained by averaging sweeping up and sweeping down curves. In low concentration (0.1 mM and 1 mM) KCl solutions, an extra dwell time of 1 s was set for each potential step in order to perform the measurement at equilibrium state. Below 0.1 mM, the conductivity of the solutions is so low that Ag/AgCl electrodes cannot respond properly.

Acknowledgements

The authors would like to thank the CMI (Center of Micro-NanoTechnology) for valuable support of microfabrication processes. We also gratefully acknowledge the CIME (Interdisciplinary Center for Electron Microscopy) for sample imaging by FIB-SEM. This work was supported by the EU research project Multiplat (FP7-NMP-2008-SMALL-2).

Notes and references

1 M. Nishizawa, V. P. Menon and C. R. Martin, *Science*, 1995, **268**, 700.
2 D. Stein, M. Kruithof and C. Dekker, *Phys. Rev. Lett.*, 2004, **93**, 035901.
3 W. Sparreboom, A. van den Berg and J. C. T. Eijkel, *Nat. Nanotechnol.*, 2009, **4**, 713.
4 R. Karnik, R. Fan, M. Yue, D. Li, P. Yang and A. Majumdar, *Nano Lett.*, 2005, **5**, 943.
5 R. Fan, M. Yue, R. Karnik, A. Majumdar and P. Yang, *Phys. Rev. Lett.*, 2005, **95**, 086607.
6 R. Karnik, K. Castelino and A. Majumdar, *Appl. Phys. Lett.*, 2006, **88**, 123114.
7 R. Fan, S. Huh, R. Yan, J. Arnold and P. Yang, *Nat. Mater.*, 2008, **7**, 303.
8 W. Guan, R. Fan and M. A. Reed, *Nat. Commun.*, 2011, **2**, 506.
9 R. Simons and G. Khanarian, *J. Membr. Biol.*, 1978, **38**, 11.
10 I. Bassignana and H. Reiss, *J. Membr. Sci.*, 1983, **15**, 27.
11 P. Ramirez, H. Rapp, S. Reichle, H. Strathmann and S. Mafe, *J. Appl. Phys.*, 1992, **72**, 259.
12 P. Ramirez, H. Rapp, S. Mafe and B. Bauer, *J. Electroanal. Chem.*, 1994, **375**, 101.
13 H. Daiguji, Y. Oka and K. Shirono, *Nano Lett.*, 2005, **5**, 2274.
14 M. E. Gracheva, J. Vidal and J.-P. Leburton, *Nano Lett.*, 2007, **7**, 1717.
15 M. E. Gracheva, D. V. Melnikov and J.-P. Leburton, *ACS Nano*, 2008, **2**, 2349.
16 R. Karnik, C. Duan, K. Castelino, H. Daiguji and A. Majumdar, *Nano Lett.*, 2007, **7**, 547.
17 H. Miedema, M. Vrouenraets, J. Wierenga, W. Meijberg, G. Robillard and B. Eisenberg, *Nano Lett.*, 2007, **7**, 2886.
18 L.-J. Cheng and L. J. Guo, *Nano Lett.*, 2007, **7**, 3165.
19 I. Vlassiouk and Z. S. Siwy, *Nano Lett.*, 2007, **7**, 552.
20 E. B. Kalman, I. Vlassiouk and Z. S. Siwy, *Adv. Mater.*, 2008, **20**, 293.
21 R. Yan, W. Liang, R. Fan and P. Yang, *Nano Lett.*, 2009, **9**, 3820.
22 M. Ali, P. Ramirez, S. Mafe, R. Neumann and W. Ensinger, *ACS Nano*, 2009, **3**, 603.
23 L.-J. Cheng and L. J. Guo, *ACS Nano*, 2009, **3**, 575.
24 E. C. Yusko, R. An and M. Mayer, *ACS Nano*, 2010, **4**, 477.
25 W.-J. Lan, D. A. Holden and H. S. White, *J. Am. Chem. Soc.*, 2011, **133**, 13300.
26 P. Mao and J. Han, *Lab Chip*, 2005, **5**, 837.
27 A. Plecis, R. Schoch and P. Renaud, *Nano Lett.*, 2005, **5**, 1147.
28 M. J. Kim, M. Wanunu, D. C. Bell and A. Meller, *Adv. Mater.*, 2006, **18**, 3149.
29 C. Dekker, *Nat. Nanotechnol.*, 2007, **2**, 209.
30 S.-W. Nam, M. J. Rooks, K.-B. Kim and S. M. Rossnagel, *Nano Lett.*, 2009, **9**, 2044.
31 G. A. Parks, *Chem. Rev.*, 1965, **65**, 177.
32 G. Parfitt, *Pure Appl. Chem.*, 1976, **48**, 415.
33 C. Martin, *Science*, 1994, **266**, 1961.
34 R. W. Mao, S. K. Lin and C. S. Tsai, *Nanotechnology*, 2009, **20**, 025301.
35 D. Crouse, Y. Lo, A. Miller and M. Crouse, *Appl. Phys. Lett.*, 2000, **76**, 49.
36 S. Shingubara, O. Okino, Y. Murakami, H. Sakaue and T. Takahagi, *J. Vac. Sci. Technol., B*, 2001, **19**, 1901.
37 L. Menon, K. Ram, S. Patibandla, D. Aurongzeb, M. Holtz, J. Yun, V. Kuryatkov and K. Zhu, *J. Electrochem. Soc.*, 2004, **151**, C492.
38 B. Yan, H. T. M. Pham, Y. Ma, Y. Zhuang and P. M. Sarro, *Appl. Phys. Lett.*, 2007, **91**, 053117.
39 H. Masuda, H. Yamada, M. Satoh, H. Asoh, M. Nakao and T. Tamamura, *Appl. Phys. Lett.*, 1997, **71**, 2770–2772.
40 I. Vlassiouk, S. Smirnov and Z. Siwy, *Nano Lett.*, 2008, **8**, 1978.